ARPS – Advanced Regional Prediction System

Center for Analysis and Prediction of Storms (CAPS)
University of Oklahoma

Army Mesoscale Modeling Forum
May 2003

Ming Xue
mxue@ou.edu

Approach

- **ARPS started in early 1990s, from scratch**
- Survey of existing models **(RAMS, MM4 later MM5, Clark, U.K. Met Office, Eta, NASA, and local models - Xue, Droegemeier, Straka).**
- Survey of advection schemes **(PPM, FCT, Smolarkiewicz, Finite volume, Finite element, Semi-Lagrangian, etc.)**
- Time integration **(mode-splitting v.s. semi-implicit)**
- Mesh refinement **(global dynamic adaptation, local refinement base on finite volume, adaptive grid nesting)**
- Equations **(compressible, nonhydrostatic, minimize approximations)**

References

- **Xue et al (1995) ARPS 4.0 User's Guide**
- **Xue et al (2000, 2001, 2003), all in Meteorology and Atmospheric Physics**
- **http://www.caps.ou.edu/ARPS**

ARPS – Coordinate System

Original equations in map-projection Cartesian coordinates

$$\frac{du}{dt} = -\frac{m}{\rho}\frac{\partial p}{\partial x} + (f + f_m)v - \tilde{f}\,w - \frac{uw}{a} + F_u \qquad \textbf{(1a)}$$

$$\frac{dv}{dt} = -\frac{m}{\rho}\frac{\partial p}{\partial y} - (f + f_m)u - \frac{vw}{a} + F_v \qquad \textbf{(1b)}$$

$$\frac{dw}{dt} = -\frac{1}{\rho}\frac{\partial p}{\partial z} - g + \tilde{f}\,u + \frac{u^2 + v^2}{a} + F_w \qquad \textbf{(1c)}$$

$$\frac{dp}{dt} = -\rho c^2 \left\{ m^2 \left(\frac{\partial u/m}{\partial x} + \frac{\partial v/m}{\partial y} \right) + \frac{\partial w}{\partial z} \right\} + \rho c^2 \left\{ \frac{\dot{\theta}}{\theta} + \frac{\dot{A}}{A} \right\}, \qquad \textbf{(1d)}$$

$$\frac{d\theta}{dt} = \frac{\dot{Q}}{C_p \pi} \qquad \textbf{(1e)}$$

$$\frac{dq}{dt} = S_q . \qquad \textbf{(1f)}$$

$$\rho = \frac{p}{R_d T}\left(1 - \frac{q_v}{\varepsilon + q_v} \right)(1 + q_v + q_{li}) \qquad \textbf{(1g)}$$

where $f_m \equiv u\frac{\partial m}{\partial y} - v\frac{\partial m}{\partial x} + u\tan(\phi)$

Coordinate System

- **The Height-based Curvilinear / Generalized Terrain-Following Coordinate**
- **Equations written in a curvilinear coordinate system (ξ, η, ζ) defined by**

$$\xi = \xi(x),\ \eta = \eta(y),\ \zeta = \zeta(x, y, z).$$

- a special case of the fully three-dimensional curvilinear system

- **Allows easy horizontal stretching and arbitrary definition of vertical grid levels as long as the lowest level follows the terrain. Flat model top is assumed (c.f. Figure)**
- **Height-based coordinate was chosen because pressure is less meaningful for small scale flows and many hi-res (e.g., radar) observations were made in height**
- **Three map projections (Polarsteographic, Lambert, Mercater) supported**

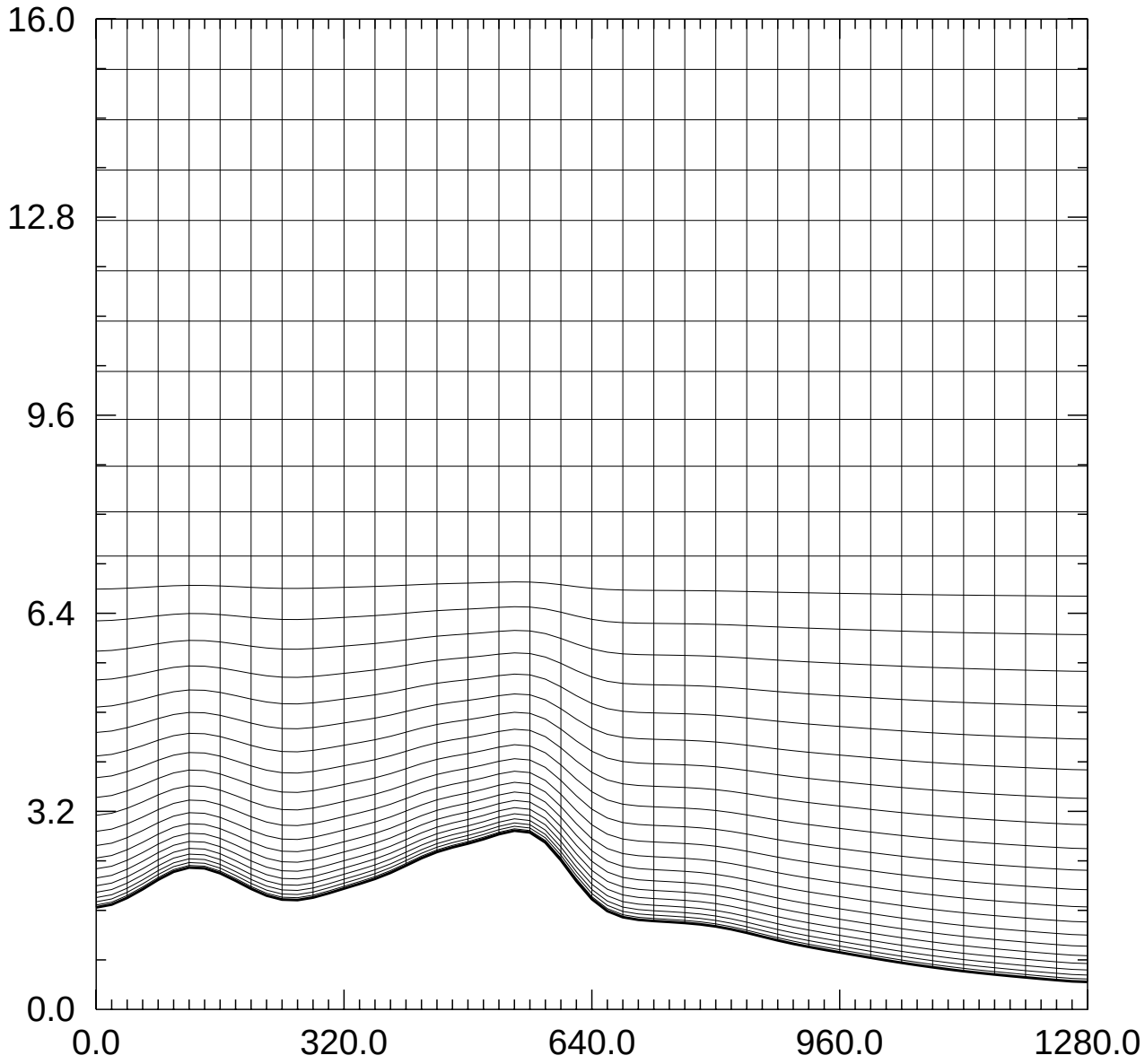
16.0
12.8
9.6
6.4
3.2
0.0
0.0
320.0
640.0
960.0
1280.0

Variables and Transformation

- Cartesian velocity *u*, *v* and *w* **instead of the** contravariant **velocity components are** used as the basic dependent variables**, so that equations can be written in a** strongly conservative form**.**
- Contravariant velocities**:**

$$U^c = uJ_3/\sqrt{G} = u/x_\xi,$$
$$V^c = vJ_4/\sqrt{G} = v/y_\eta,$$
$$W^c = (uJ_1 + vJ_2 + w x_\xi y_\eta)/\sqrt{G}.$$

- A conservation equation for scalar ϕ **is in a flux form**:

$$\left(\sqrt{G}\,\rho\phi\right)_t + \left(\sqrt{G}\,\rho U^c\phi\right)_\xi + \left(\sqrt{G}\,\rho V^c\phi\right)_\eta + \left(\sqrt{G}\,\rho W^c\phi\right)_\zeta = \sqrt{G}\,S\,\textbf{.}$$

- **Base-state + deviations:** $\varphi = \bar{\varphi}(z) + \varphi'$**.**
- **The base state is hydrostatic and is horizontally homogeneous so that their horizontal derivatives vanish.**
- **Prognostic variables: u, v, w, p', θ', q and TKE.**

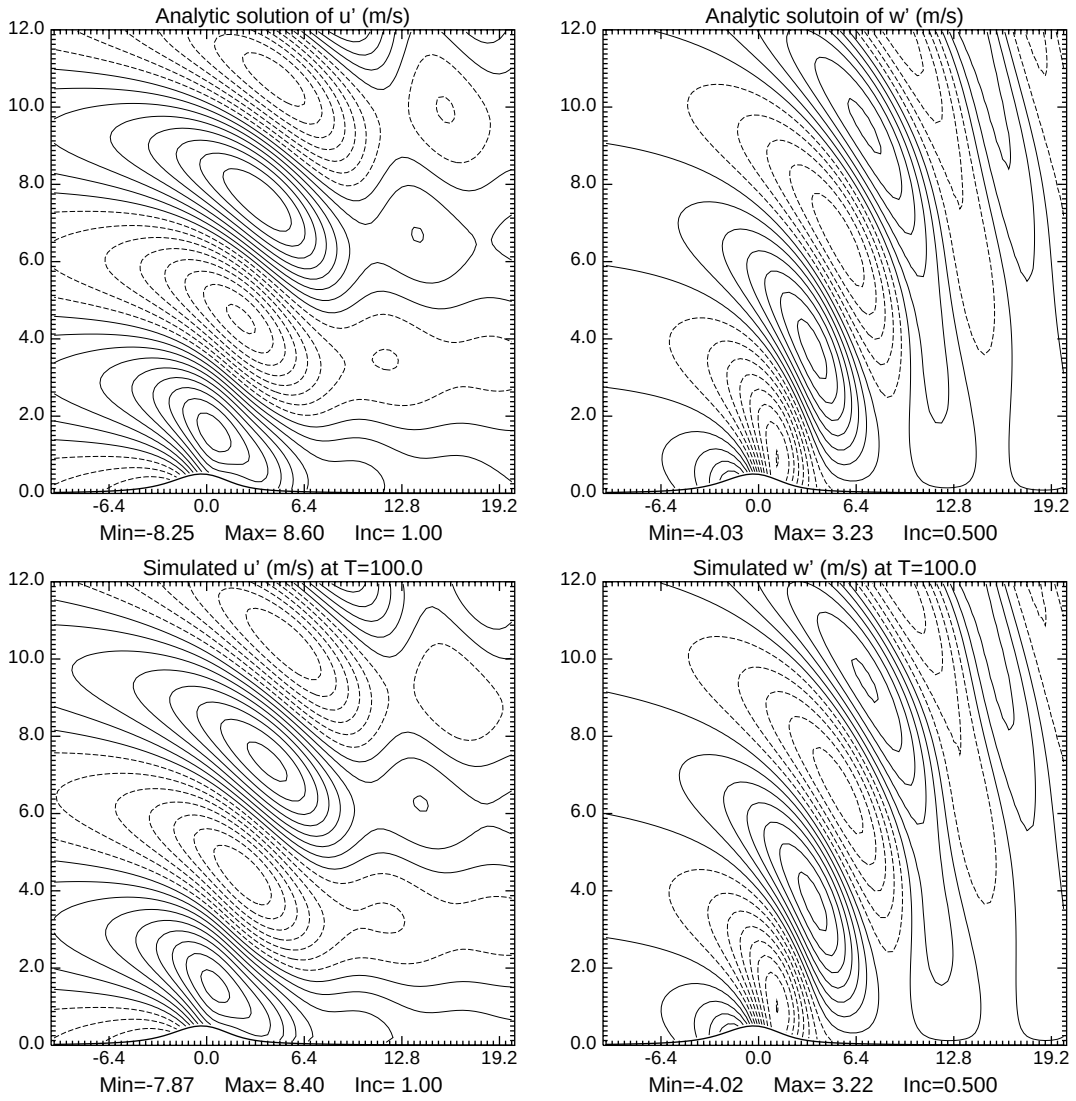

Analytical solution of u' and w' (upper panel) and model simulated solution at the ND time of 100 from experiment NLNH (lower panel) which is for finite-amplitude (nonlinear) nonhydrostatic mountain waves.

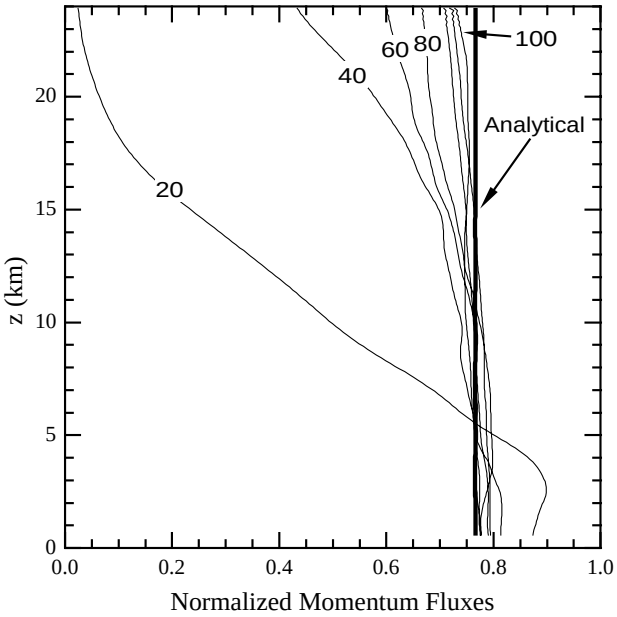

Vertical profiles of horizontal momentum at indicated ND times from experiment NLLH mountain waves.

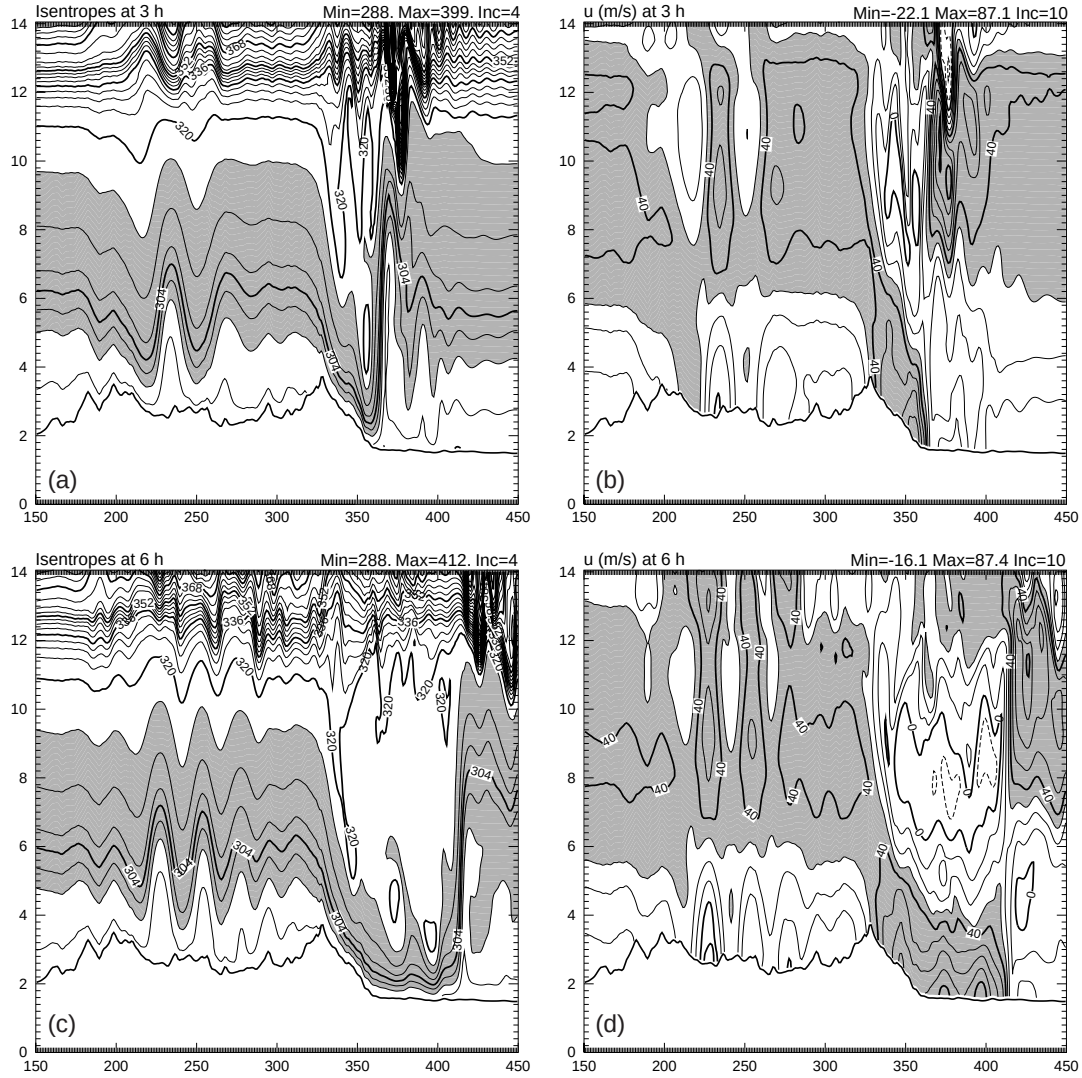

Isentropes (left panel) and u field (right panel) at hour 3 and 6 of the 2D simulation of downslope windstorm using Grand Junction, CO sounding of 1200 UTC, 11 January 1972 and a high-resolution east-west terrain profile through Boulder, CO. Regions between θ=296K and 316K one the left and where $u \geq 30$ ms^{-1} are shaded.

ARPS – Dynamic Core

Final Model Equations

$$(\rho^* u)_t + m\bar{\rho}\,\rho^{-1}\left\{\left[J_3(p' - \alpha_\xi Div^*)\right]_\xi + \left[J_1(p' - \alpha_\xi Div^*)\right]_\zeta\right\} = \tag{8a}$$
$$-ADV(u) + \rho^*\left[(f + f_m)v - \tilde{f}\,w\right] - uwa^{-1} + \sqrt{G}D_u,$$

$$\left(\rho^* v\right)_t + m\bar{\rho}\,\rho^{-1}\left\{\left[J_4(p' - \alpha_\eta Div^*)\right]_\eta + \left[J_2(p' - \alpha_\eta Div^*)\right]_\zeta\right\} = \tag{8b}$$
$$-ADV(v) - \rho^*(f + f_m)u - vwa^{-1} + \sqrt{G}D_v,$$

$$\left(\rho^* w\right)_t + \bar{\rho}\rho^{-1}\left[x_\xi y_\eta (p' - \alpha_\zeta Div^*)\right]_\zeta + g\bar{\rho}\rho^{-1}\rho^*\left[p'\left(\gamma\bar{p}\right)^{-1} - \theta'\bar{\theta}^{-1}\right] = \tag{8c}$$
$$-ADV(w) + g\bar{\rho}\rho^{-1}\rho^* B' + \rho^*\tilde{f}\,u + (u^2 + v^2)a^{-1} + \sqrt{G}D_w,$$

$$\left(\sqrt{G}p'\right)_t - \sqrt{G}\bar{\rho}gw + \rho c_s^2\left\{m^2\left[\left(\sqrt{G}U^c m^{-1}\right)_\xi + \left(\sqrt{G}V^c m^{-1}\right)_\eta\right] + \left(\sqrt{G}W^c\right)_\zeta\right\} = \tag{8d}$$
$$-\left\{m\left[\sqrt{G}U^c p'_\xi + \sqrt{G}V^c p'_\eta\right] + \sqrt{G}W^c p'_\zeta\right\} + \sqrt{G}\bar{\rho}c_s^2\left[\dot{\theta}\,\theta^{-1} + \dot{A}A^{-1}\right],$$

$$\left(\rho^*\theta'\right)_t + \rho^* w\bar{\theta}_x = -ADV(\theta') + \sqrt{G}D_\theta + \sqrt{G}S_\theta \tag{8e}$$

$$\left(\rho^* q\right)_t = -ADV(q) + \left(\rho^* V_q q / z_\zeta\right)_\zeta + \sqrt{G}D_q + \sqrt{G}S_q, \tag{8f}$$

$$\left(\rho^* E\right)_t = -ADV(E) + C + \rho^*\left[K_m\left|Def\right|^2 - 2/3E\,Div\right] - \rho^* C_\varepsilon l^{-1}E^{3/2} + 2\sqrt{G}D_E \tag{8g}$$

- **Where** $\rho^* \equiv \sqrt{G}\,\overline{\rho},\ U^* \equiv \rho^* U^c,\ V^* \equiv \rho^* V^c$ and $W^* \equiv \rho^* W^c$**.**

- **The advection operator *ADV(ϕ)* is**

$$ADV(\phi) \equiv m\left[U^* \frac{\partial \phi}{\partial \xi} + V^* \frac{\partial \phi}{\partial \eta}\right] + W^* \frac{\partial \phi}{\partial \zeta}$$

$$= m^2\left[\frac{\partial (U^*/m\phi)}{\partial \xi} + \frac{\partial (V^*/m\phi)}{\partial \eta}\right] + \frac{\partial W^* \phi}{\partial \zeta} - \phi\sqrt{G}\,Div^*$$

Notes:

- **PGF in conservative form – conserves momentum**
- **Explicit calculation of** $\frac{\partial \overline{\phi}}{\partial x}$ **and** $\frac{\partial \overline{\phi}}{\partial y}$ **avoided.**
- **Heating in pressure equation also neglected.**
- **Divergence damping damps** $\nabla \cdot (\overline{\rho}\vec{V})$ **, not** $\nabla \cdot \vec{V}$**.**
- **The series expansion for** ρ' **necessary for vertical implicit scheme retains up to second order terms in the buoyancy term**
- **Physical mixing done in physical coordinates**

Solution method

- **Arakawa C-grid**

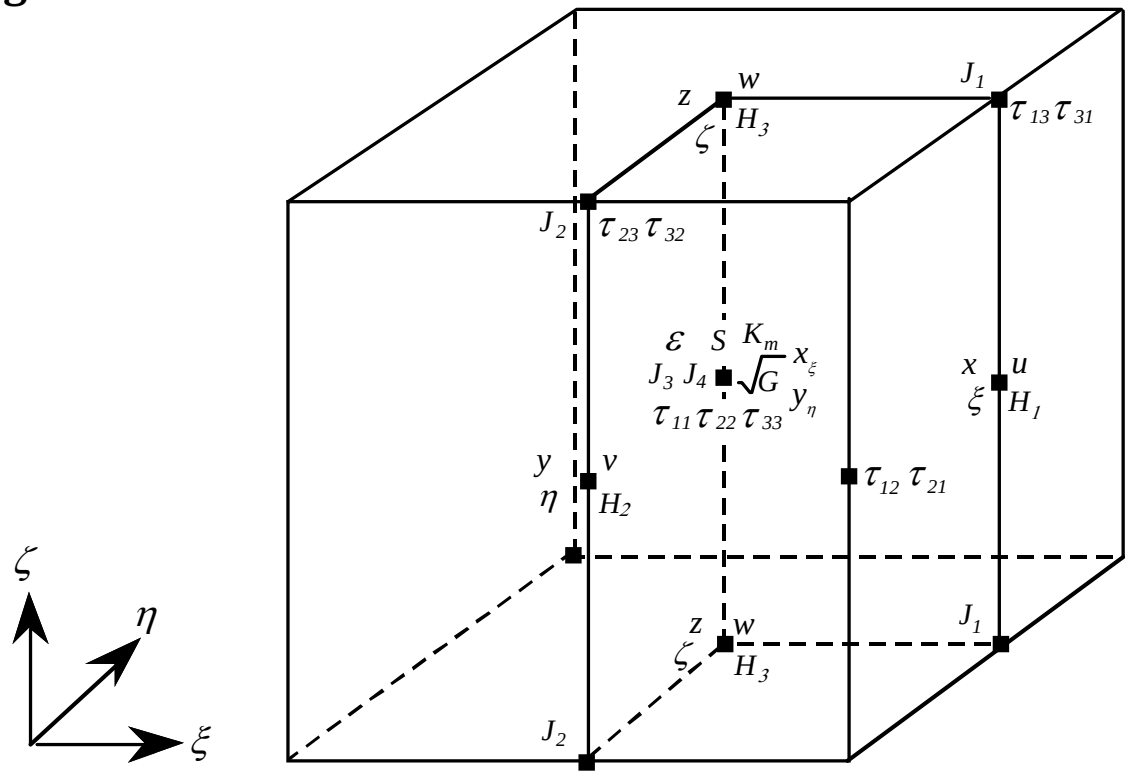

A schematic depicting the staggering of variables on a grid box. The derived quantities are located so as to minimize spatial averaging in the finite difference calculations.

Solution Method

- Advection**: Fourth-order and second-order quadratically conservative form – conserves 1st and 2nd moments.**
- 2nd-order and 4th-order monotonic Flux-corrected transport (**FCT**) and positive definite **MDPDC options for scalars.**
- **2nd, 4th and 6th-order computational mixing with monotonic option for the high orders**
- Mode-splitting time integration
  - **Implicit for acoustic modes in the vertical.**
  - **Option to include gravity wave mode in small time steps.**
- **Horizontal domain decomposition via MPI**
- **Dynamic memory allocation with F90**

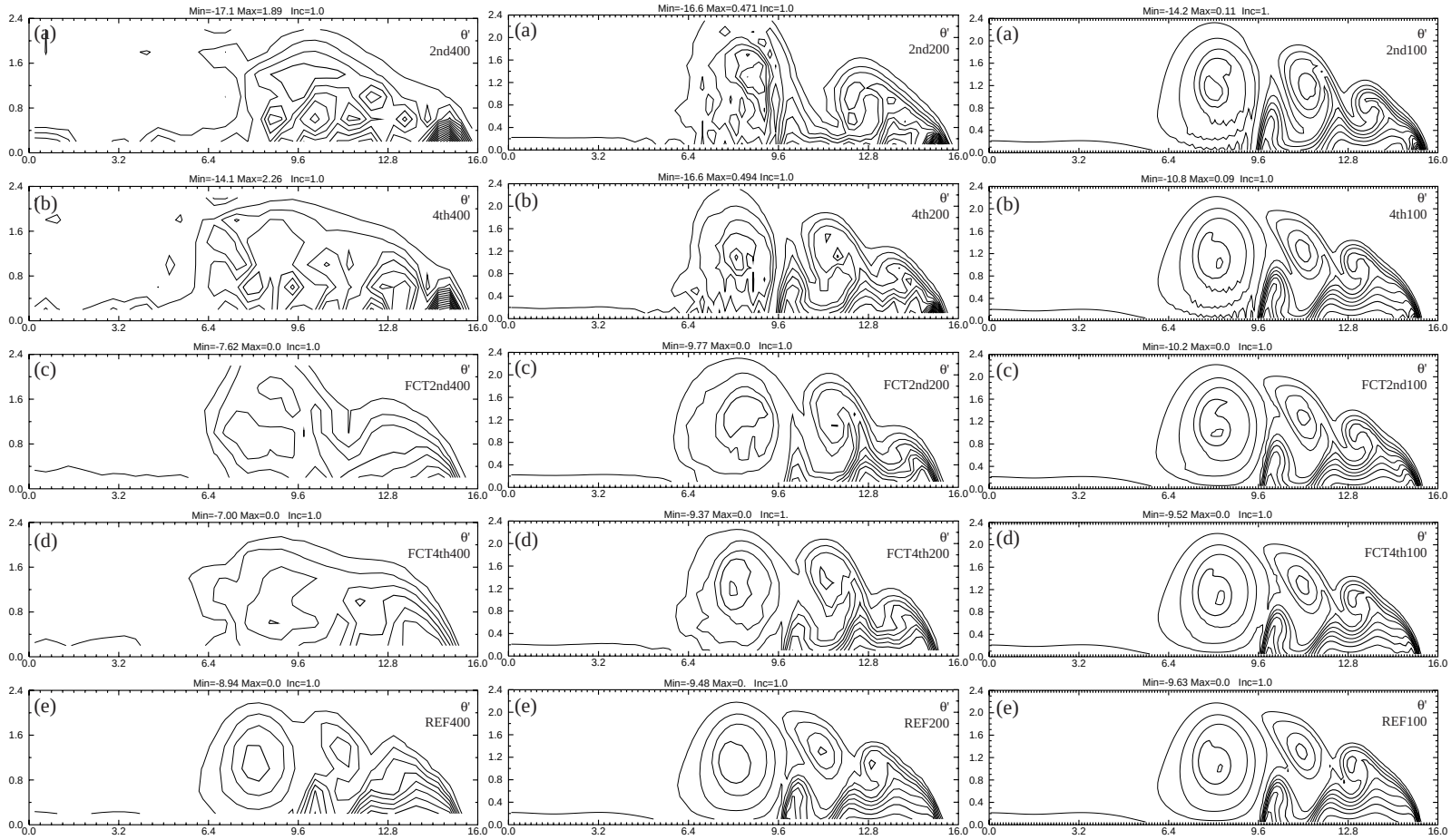

Fields of θ' at 900 s @ 400, 200 and 100 m resolutions (a) 2nd400, (b) 4th400, (c) FCT2nd400, (d) FCT4th400 and (e) the 25 m reference run. The reference solution has been averaged to the corresponding resolutions.

Effects of Advection Schemes on Supercell Storm Rainfall

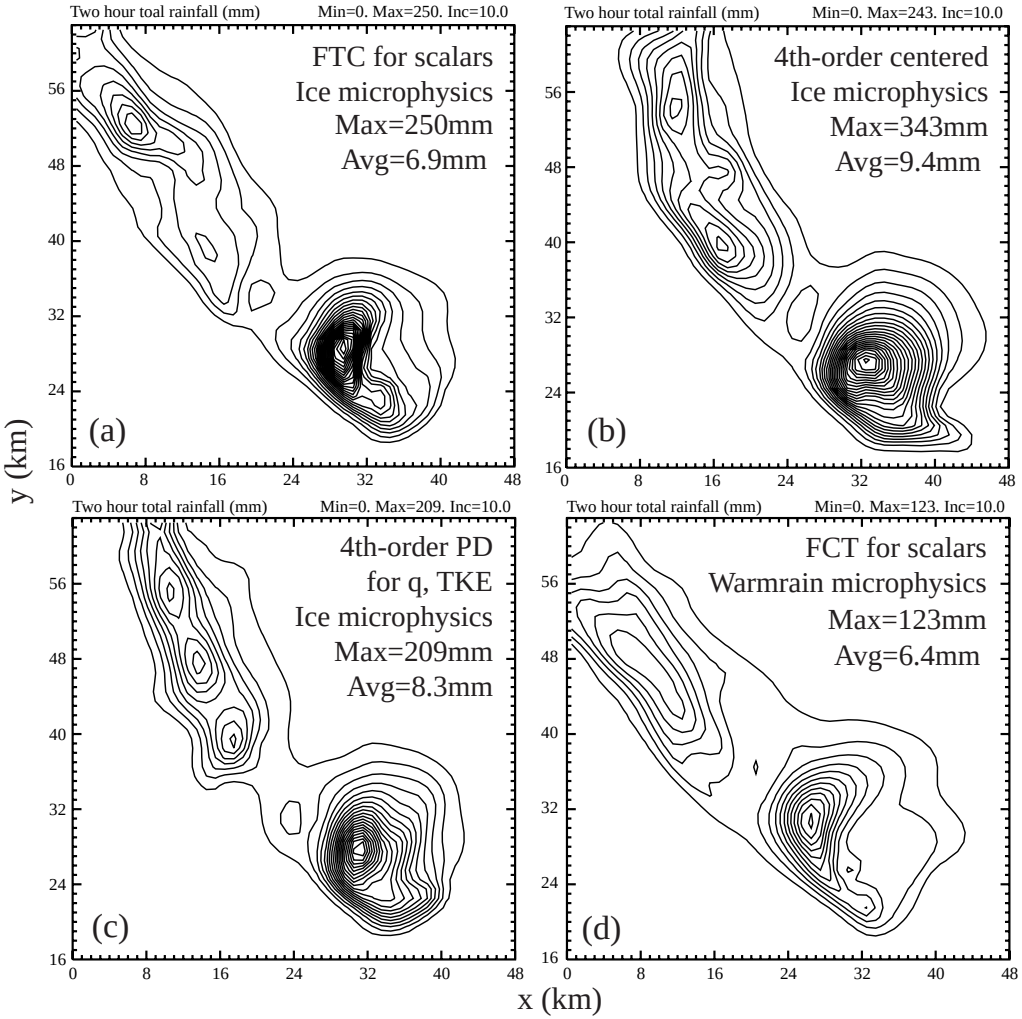

ARPS – Subscale Fluxes

Turbulence, boundary layer and land surface models

- **Monotonic high-order computational mixing (Xue 2000)**
- **Three-dimensional subgrid-scale turbulence parameterization**
  - **1.5-order TKE scheme**
  - **Smagorinsky**
  - **Germano (for LES modeling only)**
- **Anisotropic turbulence formulation when $\Delta x >> \Delta z$.**
- **PBL parameterization based on 1.5-order TKE scheme (Sun and Chang 1986) – mixing length related to convective PBL depth**
- **Vertical mixing handled implicitly.**
- **Stability-dependent similar-theory based surface fluxes + evapotranspiration flux from LSM**
- **Two-layer force-restore type (Noilhan and Planton and later improvements) and multi-layer soil-vegetation model similar to NOAH**
- **Multiple soil types allowed in each grid cell**

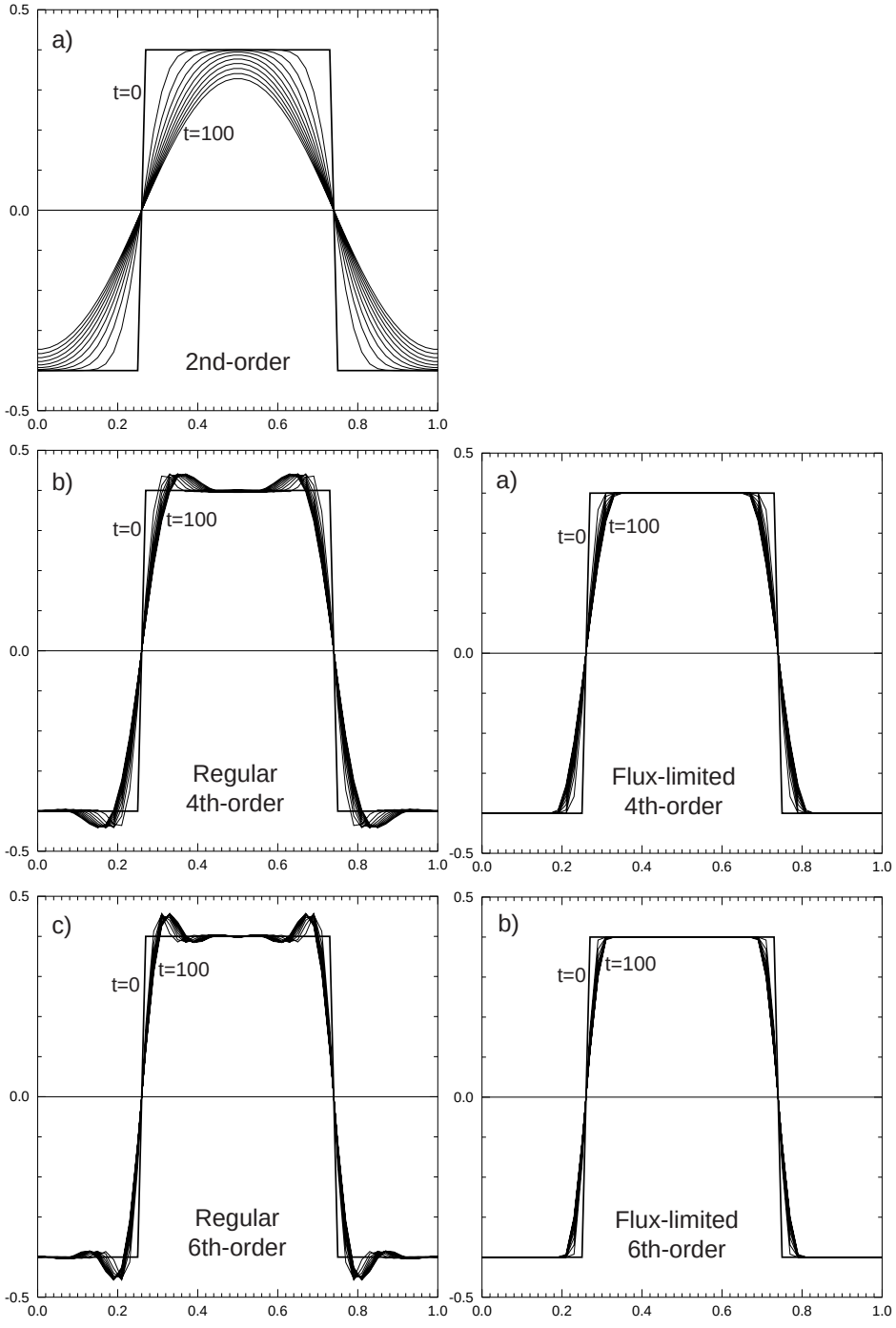
a)
t=0
t=100
2nd-order
b)
t=0
t=100
Regular
4th-order
a)
t=0
t=100
Flux-limited
4th-order
c)
t=0
t=100
Regular
6th-order
b)
t=0
t=100
Flux-limited
6th-order
0.5
0.0
-0.5
0.0
0.2
0.4
0.6
0.8
1.0

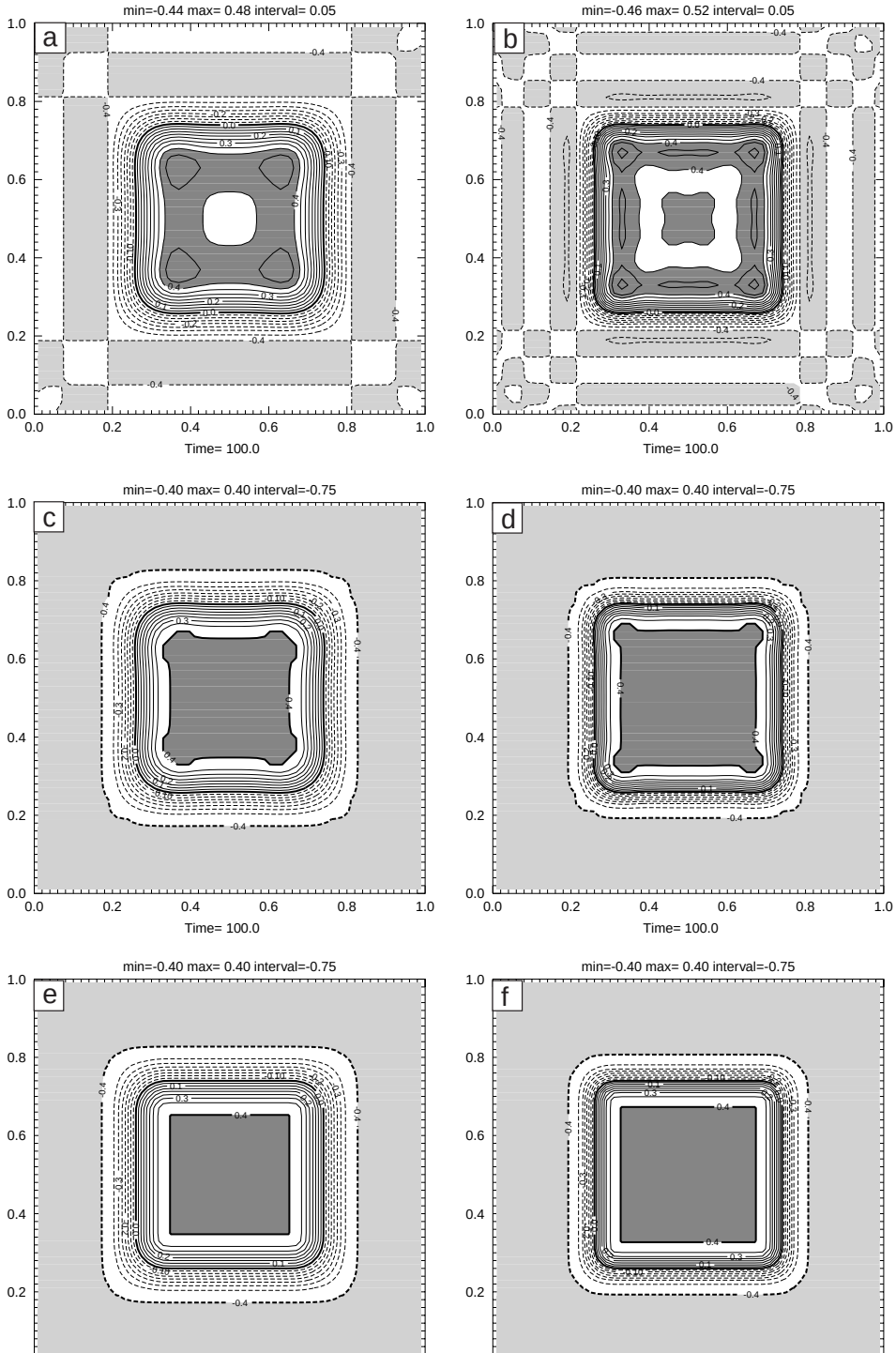
min=-0.44 max= 0.48 interval= 0.05
a
Time= 100.0
min=-0.46 max= 0.52 interval= 0.05
b
Time= 100.0
min=-0.40 max= 0.40 interval=-0.75
c
Time= 100.0
min=-0.40 max= 0.40 interval=-0.75
d
Time= 100.0
min=-0.40 max= 0.40 interval=-0.75
e
min=-0.40 max= 0.40 interval=-0.75
f

Figure 1. Contour maps of a 2D field after subjecting to regular 4^{th}-order (a), regular 6^{th}-order (b), 4^{th}-order flux-corrected (c), 6^{th}-order flux-corrected (d), 4^{th}-order with simple flux limiter (e) and 6^{th}-order with simple flux limiter (f) diffusion schemes for 100 time steps at time 100. The plotting conventions are the same as in Fig.5 (From Xue 2000).

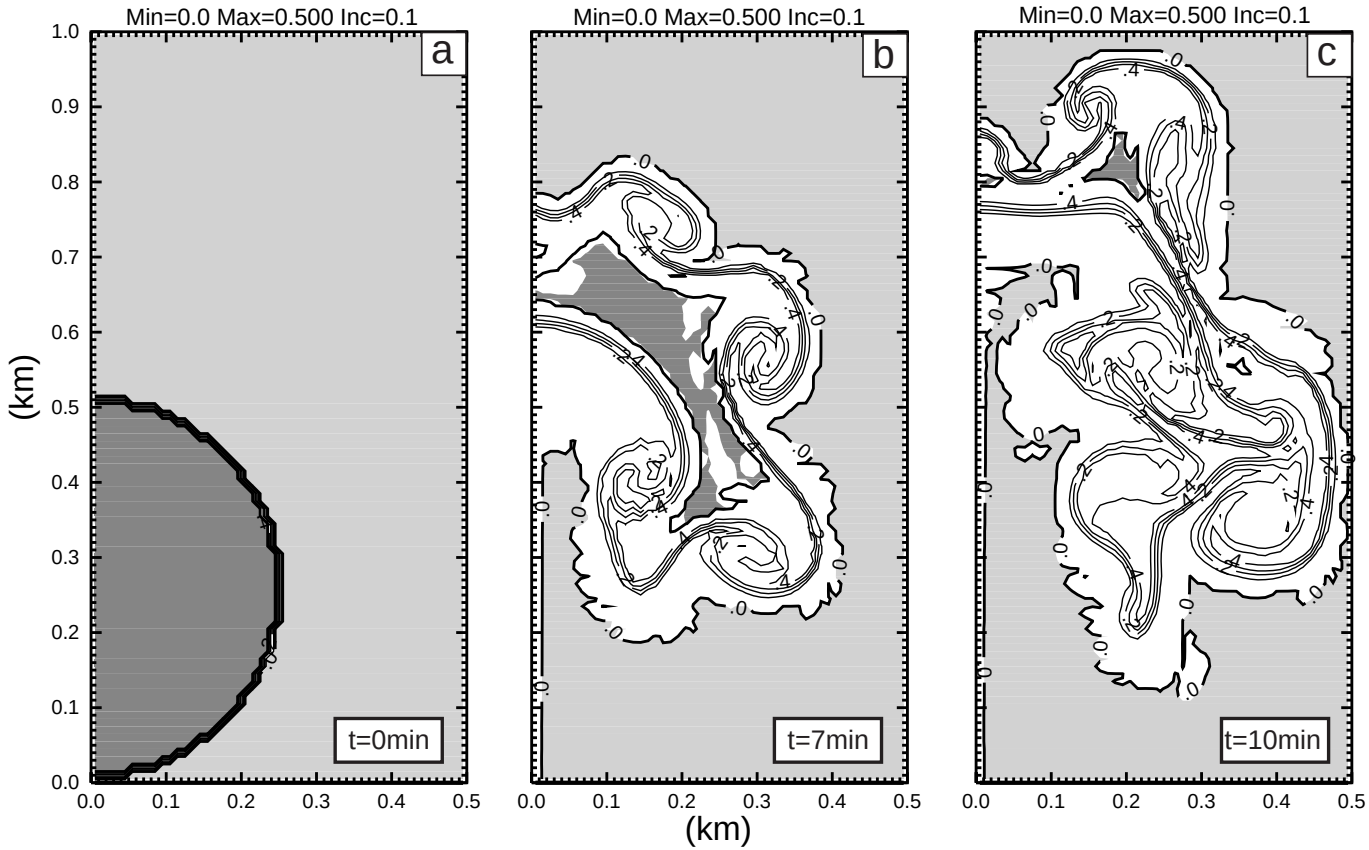

Figure 2. Perturbation potential temperature (θ') fields at t=0 min (a), t=7 min (b), and t=10 min (c), showing the evolution of a thermal bubble in a neutral environment. Flux-corrected transport is used for potential temperature advection and the *simple* flux-limited (monotonic) 6^{th}-order diffusion is applied to momentum. Zero and 0.5 contours are thickened, and areas with values equal to or greater than 0.5 are indicated by dark shading whereas areas with values equal to or less than 0.0 are represented by light shading. Hardly any undershooting or undershooting exists in

the solution as indicated by the maximum and minimum values in the plots, due to the use of monotonic FCT advection and the absence of non-monotonic diffusion (From Xue 2000).

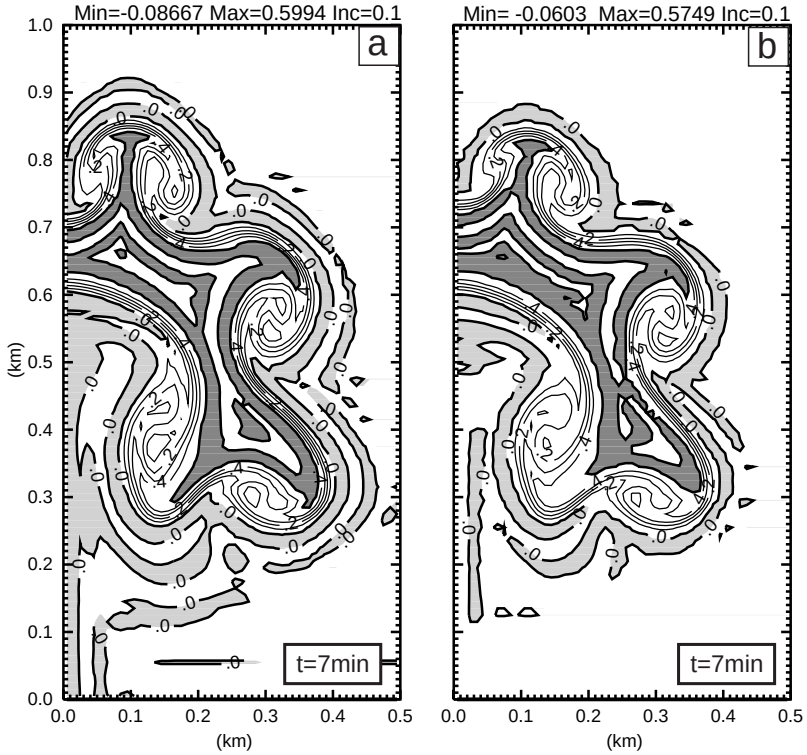

Figure 3. As in Fig.8, except in (a) regular 6th-order diffusion and in (b) simple monotonic 6th-order diffusion is used. Again, undershooting and overshooting are smaller in the (b) where monotonic 6th-order diffusion is used (From Xue 2000).

Subgrid-scale turbulence parameterization

$$D_{u_i} = m\left[(\tau_{i1})_x + (\tau_{i2})_y\right] + (\tau_{i3})_z,$$

$$\tau_{ij} = \bar{\rho} K_{mj} D_{ij}, \qquad D_{ij} = m_i m_j m_k \left\{\left[u_i/(m_j m_k)\right]_{x_i} + \left[u_j/(m_i m_k)\right]_{x_j}\right\}$$

$$D_\phi = m\left[(H_1)_x + (H_2)_y\right] + (H_3)_z,$$

$$H_j = \bar{\rho} K_{Hj} m_j (\phi)_{x_j},$$

a) The 1.5-order TKE-based turbulence closure

$$K_{mj} = 0.1\, E^{1/2}\, l_j .$$

$$l_1 = l_2 = l_3 = \begin{cases} \Delta & \text{for unstable or neutral case} \\ \min(\Delta, l_s) & \text{for stable case} \end{cases}$$

where $\Delta = (\Delta x\, \Delta y\, \Delta z / m^2)^{1/3}$ and $l_s = 0.76 E^{1/2} N^{-1}$.

Anisotropic turbulence,

$$l_1 = l_2 = \Delta_h \text{ and } l_3 = \begin{cases} \Delta_v & \text{for unstable or neutral case} \\ \min(\Delta_v, l_s) & \text{for stable case} \end{cases}$$

$$\mathrm{Pr} = \max\left[1/3, \left(1 + 2l_3/\Delta_v\right)^{-1}\right],$$

The non-local PBL parameterization

- **The turbulence closure schemes are designed to parameterize the local mixing due to *sub-grid scale* turbulence. In a convectively unstable boundary layer, most of the vertical mixing is achieved by 'large' boundary layer eddies (Wyngaard and Brost, 1984).**

- **Unless the vertical as well as the horizontal resolutions of the model are on the order of 100 m or less so as to resolve most of the boundary layer eddies (100 m or less), additional parameterization is necessary.**

- **The treatment of convective boundary layer turbulence is a combination of the 3-D, 1.5-order Deardorff SGS turbulence scheme and an ensemble turbulence closure scheme of Sun and Chang (1986).**

- **The vertical turbulent mixing length l_3 is related to the (non-local) PBL depth instead of the local vertical grid spacing inside an unstable PBL.**

  $$l_3 = l_0\{1.8z_i[1-\exp(-4z/z_i)-0.0003\exp(8z/z_i)]\},$$

  where z is the height above ground and z_i the top of PBL.

- **Under stable conditions or above the convective boundary layer, the length scale l reverts back to that of the Deardorff scheme**

- **PBL parameterization versus explicit mixing via large eddies (Xue et al 1996)**

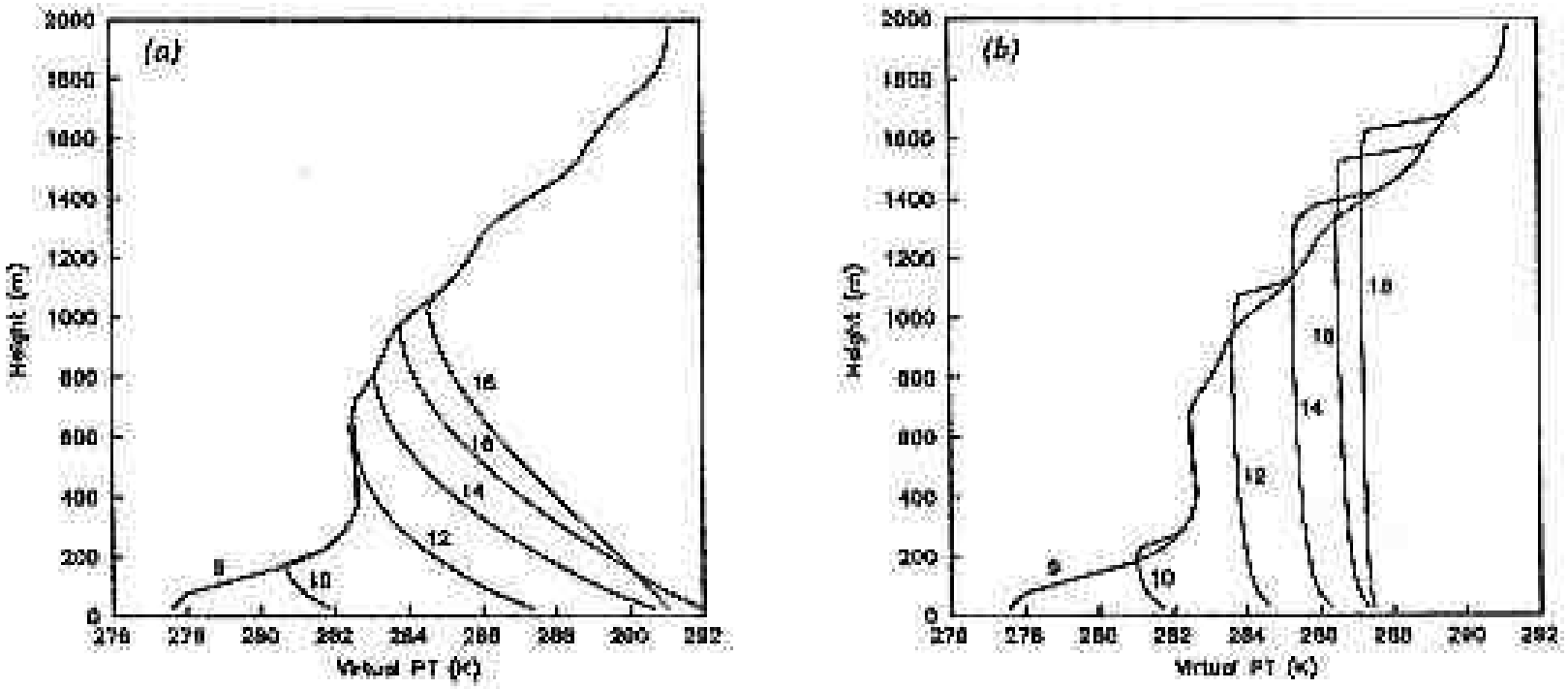

Profiles of θ_v from 1-D experiments with Deardorff SGS turbulence (a) and Sun and Chang PBL scheme (b), for Wangara day-33 case

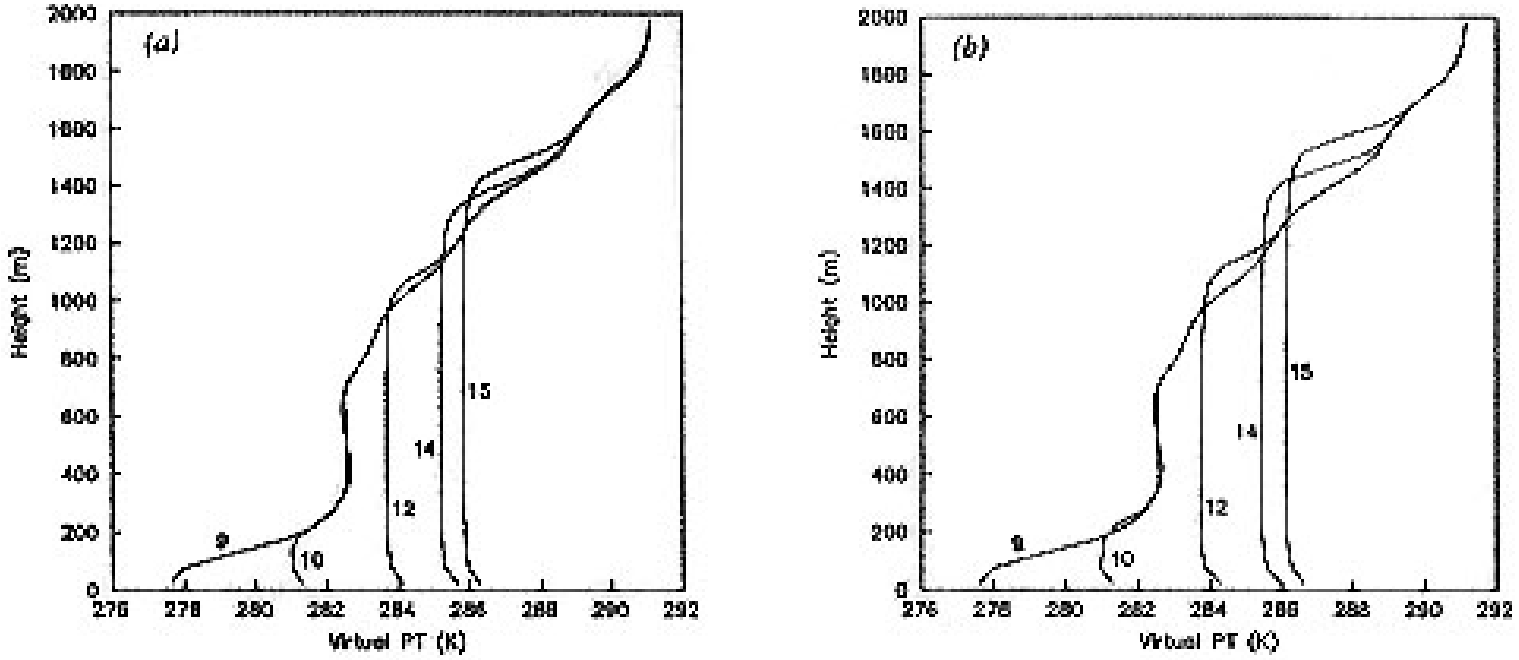

Profiles of θ_v from 3-D experiments at dx=125m with Deardorff SGS turbulence (a) and Sun and Chang PBL scheme (b)

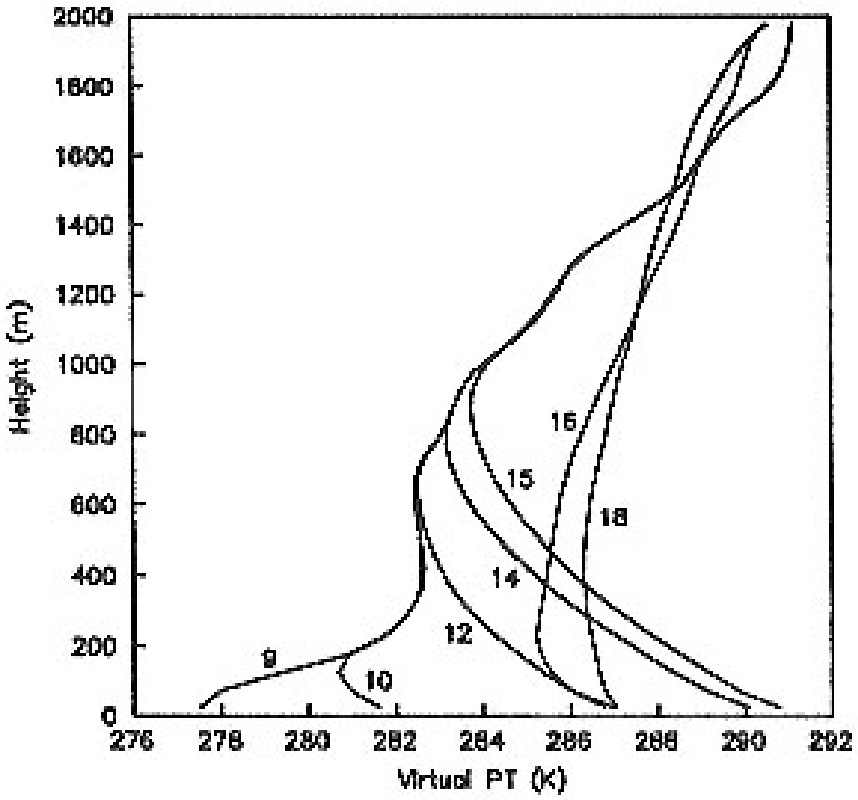

Profiles of θ_v from 3-D experiments at dx=6km with Deardorff SGS turbulence (b)

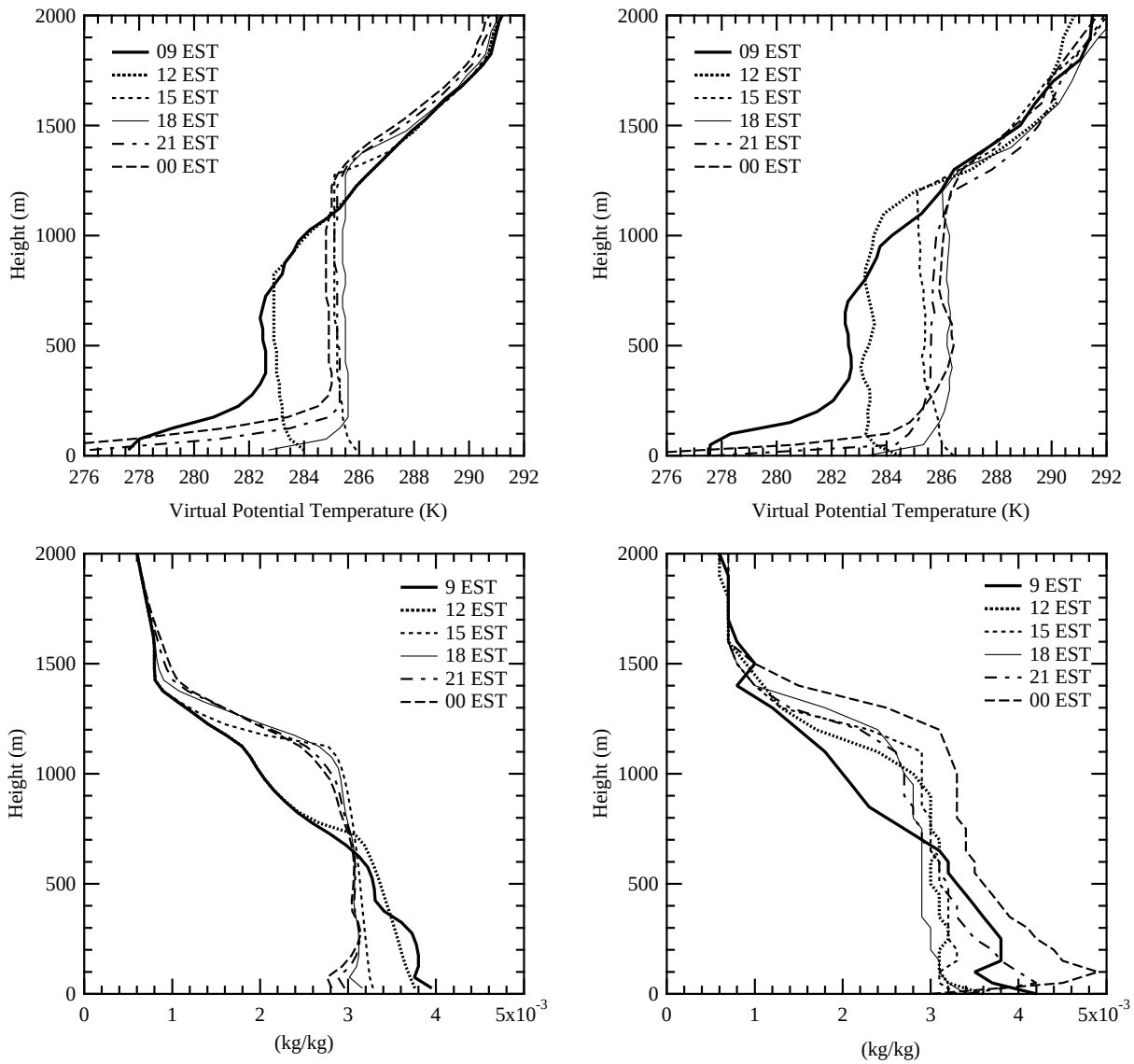

Profiles of virtual potential temperature, θ_v, (upper panel) and specific humidity, q_v, (lower panel) simulated by coupled ARPS runs (left panel) and from Wangara Day 33 data (right panel)

Verification of Multi-layer Land-surface model (OUsoil) against OK Mesonet Soil data

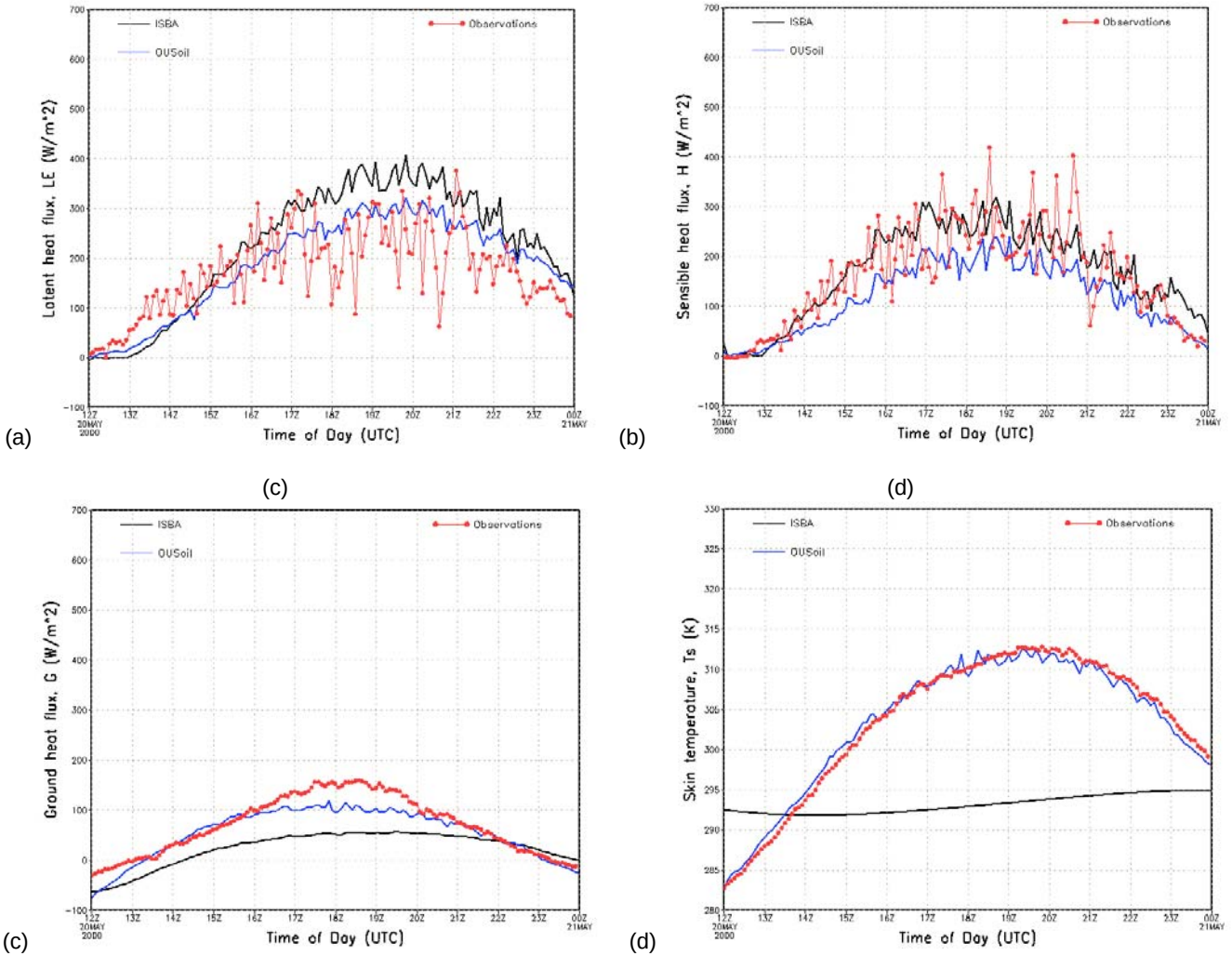

Model output for the ISBA and OUSoil LSMs plotted against observations collected at NORM during 20 May, 2000. Data include a) latent heat, b) sensible heat, and c) ground heat fluxes (W m^{-2}), and d) skin temperature (°K).

Table 1: Statistics of the differences between the ISBA and OUSoil scheme results and Mesonet observations. The root-mean-square difference (RMSD), the mean absolute percent difference (MAPD), and the mean bias (MB) were estimated for each site for each day examined.

		RMSD (W m^{-2})/(K)		MAPD (W m^{-2})/(K)		MB (W m^{-2})/(K)	
		ISBA	OUSoil	ISBA	OUSoil	ISBA	OUSoil
May 20, 2002							
NORM	LE	11.6	4.7	44.5	30.2	50.9	15.4
	H	27.2	12.3	25.2	31.7	9.1	-43.6
	G	32.6	44.8	69.8	27.0	-46.0	-15.6
	Ts	9.76	0.11	3.9	0.3	-10.4	-0.0
	Rn-H-LE-G	85.9	65.33			-15.6	42.4
BURN	LE	326.7	148.9	245.4	113.4	272.9	119.9
	H	168.4	162.6	56.6	59.7	-124.6	-141.3
	G	49.5	27.6	59.7	58.7	29.4	21.1
	Ts	14.3	11.0	4.1	3.0	-12.9	-9.5
	Rn-H-LE-G	168.2	46.2			-139.0	39.1
Aug 1, 2002							
NORM	LE	76.9	56.7	27.9	20.0	15.7	-40.1
	H	52.9	36.5	33.1	21.9	21.9	9.6
	G	30.4	35.2	56.8	54.6	-18.2	-22.8
	Ts	2.02	3.32	0.6	0.8	-1.27	1.73
	Rn-H-LE-G	107.3	69.2			-15.1	57.5
Aug 2, 2002							
BURN	LE	3.3	5.1	39.7	22.3	-109.5	-31.1
	H	166.9	33.5	166.5	29.3	137.9	-17.3
	G	81.1	47.8	155.0	73.2	25.0	11.4
	Ts	1.12	1.36	0.4	0.9	-1.26	-2.62
	Rn-H-LE-G	125.3	53.8			-54.1	36.3

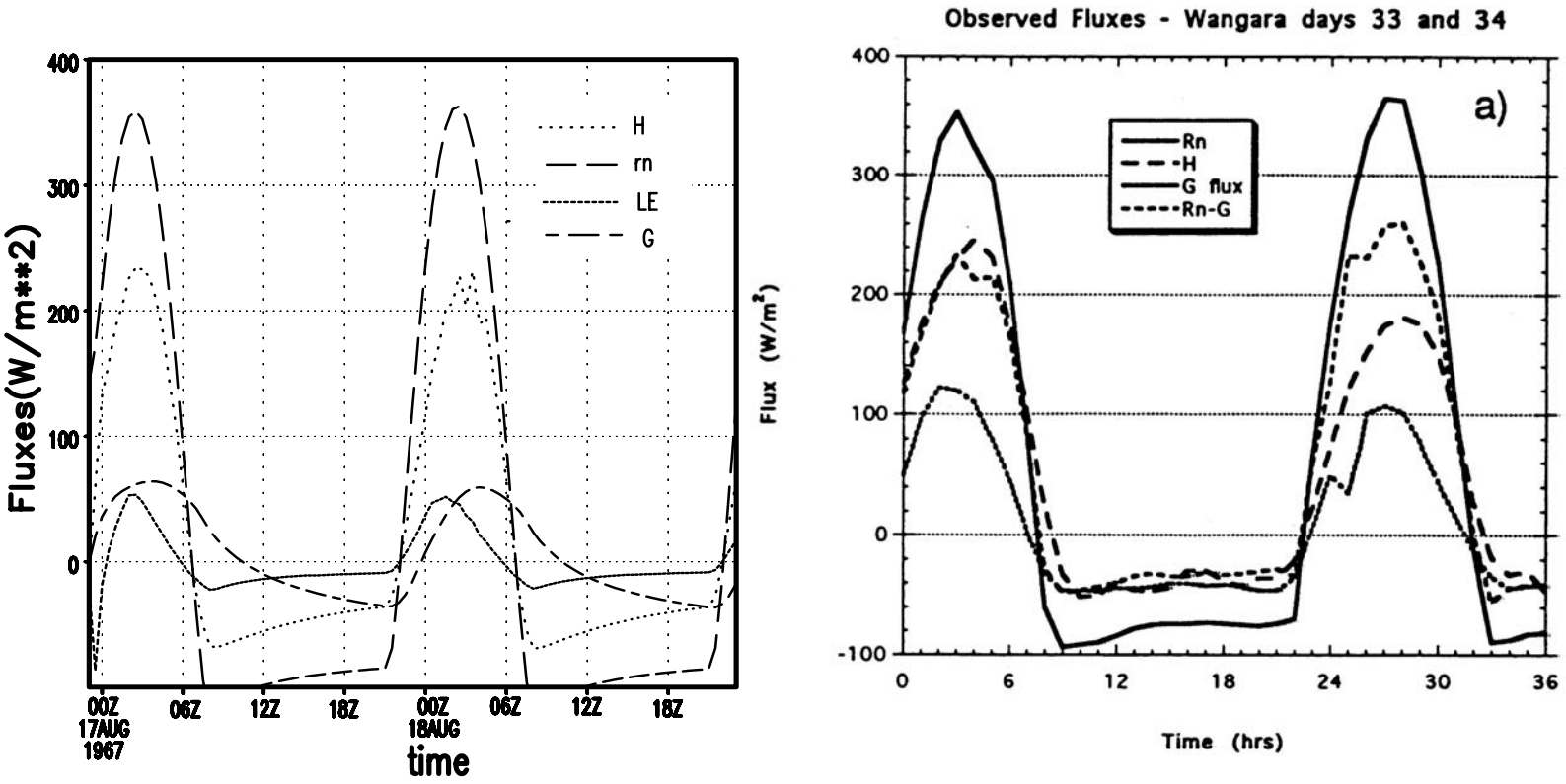

The simulated (a) and observed (b) surface fluxes of net radiation (R_n), sensible heat (H), latent heat (LE), and ground heat (G) for Wangara days 33 and 34. 0Z corresponds to 9 am local time.